Characterization and reduction of reabsorption losses in luminescent solar concentrators

Lindsay R. Wilson,[1] Brenda C. Rowan,[1] Neil Robertson,[2] Omar Moudam,[2] Anita C. Jones,[2,3] and Bryce S. Richards[1,4]

[1]School of Engineering and Physical Sciences, Heriot-Watt University, Edinburgh EH14 4AS, U.K.

[2]School of Chemistry, University of Edinburgh, King's Buildings, West Mains Road, Edinburgh EH9 3JJ, U.K.

[3]a.c.jones@ed.ac.uk

[4]b.s.richards@hw.ac.uk

Received 12 January 2010; accepted 1 February 2010;
posted 19 February 2010 (Doc. ID 122571); published 16 March 2010

The effects of excitation wavelength on the optical properties (emission spectrum and quantum yield) of a luminescent solar concentrator (LSC) containing a fluorescent organic dye (Lumogen F Rot 305) are studied. Excitation at wavelengths on the long-wavelength edge of the absorption spectrum of the dye results in redshifted emission, but the quantum yield remains constant at 100%. The origin of this effect and its consequences are discussed. The extent of the long-wavelength tail of the absorption spectrum of the dye is determined and the importance in reabsorption losses is shown. The optical efficiencies and photon transport probabilities of LSCs containing either an organic dye or a rare-earth lanthanide complex are compared using ray-tracing simulations and experiment. The optical efficiency is shown to depend strongly on the Stokes shift of the fluorophore. The lanthanide complex, which has a very large Stokes shift, exhibits a higher optical efficiency than the dye (64% cf. 50%), despite its lower quantum yield (86% cf. 100%).

OCIS codes: 260.2510, 300.6280, 250.5460, 350.6050.

1. Introduction

Luminescent solar concentrators (LSCs) [1–5] were proposed more than 30 years ago [5] as a nonimaging means of concentrating solar radiation. They use a sheet of transparent material, such as glass or plastic, doped with fluorophores, such as organic dyes, quantum dots, or rare-earth complexes. Sunlight is absorbed by the doped sheet and a fraction of the fluorescence is trapped by total internal reflection (TIR) due to the difference in refractive indices at the LSC–air interface. Light is transported to the edges of the sheet, where it is collected by solar cells, by successive internal reflections. The LSC is the only concentrating photovoltaic technology that can harvest all diffuse components of sunlight, as well as the direct component, which is an important consideration for operation in the cloudier climates of northern Europe. In addition, since the spectrum of light incident on the edge-mounted solar cells contains far more favorable wavelengths of light for photovoltaic conversion, the solar cells operate at lower temperatures. With some of the excess photon energy being deposited in the LSC, rather than in the cells, this leads to higher cell efficiencies [5,6].

Numerous different fluorophores have been developed and tested for use in LSCs, including organic dyes [7–9], quantum dots [10–13], and rare-earth materials [14–16]. However, a problem common to both organic dyes and quantum dots is the effect of reabsorption resulting from an overlap of their absorption and emission spectra. Reabsorption occurs when first-generation fluorescence photons, which are trapped inside a LSC sheet, are absorbed by another molecule of the same dye. When this happens, two loss mechanisms occur. First, if the dye has

0003-6935/10/091651-11$15.00/0

nonunity photoluminescent quantum yield (PLQY), then there is a chance that a second-generation fluorescence photon will not be emitted. Second, even if a second-generation fluorescence photon is produced, there is an additional large probability that it will be emitted at less than the critical angle and lost through what is known as the escape cone of the sheet. The probability of the emitted photon being trapped inside the sheet at each emission event is given by

$$P_{\mathrm{TIR}} = \frac{\sqrt{n^2 - 1}}{n}, \tag{1}$$

where n is the refractive index of the sheet material. For a sheet with $n = 1.49$, such as polymethyl methacrylate (PMMA), $P_{\mathrm{TIR}} = 74\%$. It has been reported that reabsorption is one of the major limiting factors in LSC development [17,18].

Several approaches have been proposed to deal with reabsorption [19], such as altering the host material [20,21], hot mirrors [22], and directionally emitting dyes [23]. A recent approach has been the development of rare-earth complexes that exhibit zero overlap of their absorption and emission spectra. Such complexes contain absorbing organic ligands and emitting rare-earth ions, such as europium, ytterbium, and neodymium [24]. Because of the energy transfer mechanism between their absorbing ligands and emitting ions [25,26], they can exhibit large Stokes shifts. These complexes absorb in the ultraviolet (UV) or visible and emit in the red or near-infrared (NIR).

In this paper, the effects of reabsorption and spectral overlap on photon transport in LSC devices are studied using a combination of Monte Carlo ray-tracing simulations and experiment. The optical properties of an organic dye (BASF Lumogen F Rot 305) in a LSC have been measured over a range of excitation wavelengths, and the emission spectrum is found to depend on the excitation wavelength, when exciting at wavelengths on the long-wavelength edge of the absorption spectrum. This observation is contrary to the general assumption [27–31] in modeling of LSC performance that, since the emission process of an excited organic dye molecule is independent of excitation wavelength (Kasha's rule [32]), the emission spectrum and PLQY of the dye-doped LSC are also independent of excitation wavelength. The origin of this effect and its implications in the prediction of reabsorption losses in LSC are discussed. Measurements of fluorescence spectra from the end of a strip sample of LSC material under point excitation reveal how the photon transport probability varies with path length. It is also shown that such emission spectra can be used to determine the long-wavelength tail of the absorption spectrum of the organic dye. Finally, simulations of a square LSC module under uniform illumination show the effects of reabsorption and host absorption on photon transport, and these are confirmed experimentally.

2. Experimental

A. Properties of the Fluorophores

Two fluorophores with widely different Stokes shifts were chosen for this study. Lumogen F Rot 305 (termed R305), is an organic perylene dye manufactured by BASF [33–35], which was developed to have a high PLQY, broad absorption range, and good photostability for use in LSCs [7]. The other (termed EuhD) is a ligand-sensitized rare-earth (RE) complex, developed at the University of Edinburgh, that contains europium as the emitting ion [24]. The structure and energy-level diagrams of both EuhD and R305 are shown in Fig. 1.

The europium ion is complexed with a hexafluoroacetylacetone (hfac) ligand and a bis(2-(diphenylphosphino)phenyl) ether oxide (DPEPO) coligand, giving the formula $\mathrm{Eu(hfac)_3}$ (DPEPO). This particular ligand arrangement gives rise to an absorption peak at 300 nm. Light energy absorbed by the ligands is transferred to the ligand triplet state via intersystem crossing (ISC) and then by resonance energy transfer to the europium ion [Fig. 1(a)] [36]. The europium emission occurs in five narrow bands at 578, 592, 613, 650, and 697 nm, corresponding to the $^5\mathrm{D}_0 \rightarrow {}^7\mathrm{F}_{J=0,1,2,3,4}$ transitions, with the main peak at 613 nm. Although this particular RE complex is not ideal for LSC design as the absorption range only covers the UV region, its purpose in this paper is to demonstrate the potential advantages of RE complexes, in particular the large Stokes shifts.

The small (30 nm) Stokes shift of R305 is a feature of nearly all organic dyes [24,32], which, therefore, exhibit significant reabsorption when implemented in a LSC. By contrast, EuhD absorbs only in the UV region of the spectrum and emits in the red region, with a Stokes shift of 320 nm. There is zero spectral overlap and no possibility of reabsorption occurring.

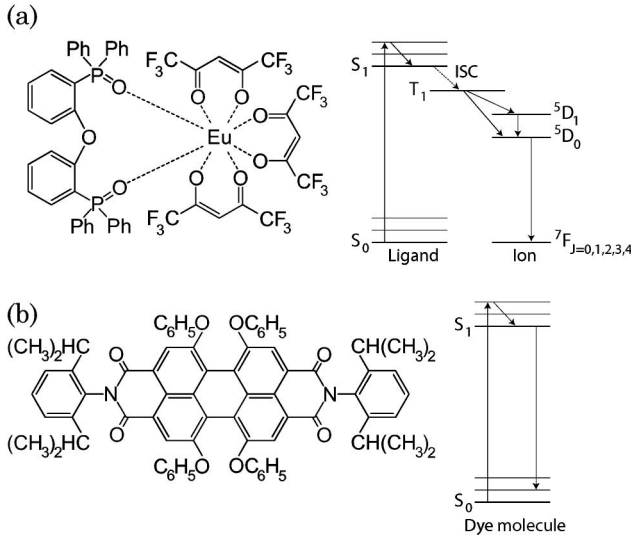

Fig. 1. Structure and energy-level diagrams of (a) EuhD [24] and (b) R305 [7]. The absorption and emission processes for each fluorophore are indicated.

Absorption and emission spectra for both R305 and EuhD, measured in PMMA hosts, are shown in Fig. 2. When measuring the emission spectrum of R305, a low concentration [5 parts per million (ppm)] was used in conjunction with excitation and detection at the edge of the sample to minimize the effects of reabsorption on the shape of the emission spectrum.

An integrating sphere technique [37] was used to measure the PLQY of both R305 and EuhD in PMMA at excitation wavelengths of 530 and 320 nm. Values obtained were $100 \pm 1\%$ [37] for R305 and $86 \pm 5\%$ [24] for EuhD.

B. Sample Preparation

The fluorophores were cast into PMMA sheets by a standard thermal polymerisation technique [38]. Casting syrup was made by dissolving 10 wt. % PMMA polymer powder in methyl methacrylate monomer (both from Lucite International). The required mass of dye was then dissolved in this syrup and the mixture polymerized in a glass-plate mold with 0.08 wt. % azobisisobutyronitrile initiator using a water bath. After postcuring in a hot-air oven, residual monomer content was below 0.3 wt. %, as measured by gas chromatography. The sample thickness was 3 ± 0.1 mm.

Rectangular sample strips (10 cm × 1.2 cm) were cut from the cast sheets. Both long edges and one short edge were roughened and coated with matte black paint to stop internal reflections from these surfaces. Square (10 cm × 10 cm) sheets were also cut and their edges were finished with a diamond edge polisher. Sample concentrations (both for strip and square samples) are listed in Table 1.

C. Measurement of Edge Emission as a Function of Excitation Distance

To measure the edge-emitted spectrum of the strip samples at different excitation distances from the edge, a setup similar to that used by Sansregret *et al.* [39] and Earp *et al.* [40] was used. This is shown in Fig. 3.

The experiment was designed to closely approximate a point excitation source with a straight-line path of the emission to the edge and minimal fluorescence from locations other than the excitation spot. This is achieved by using narrow strips with blackened edges, ensuring that any fluorescence detected arises primarily from the point of excitation with minimal contributions from edge reflections.

The 10 cm × 1.2 cm strip of fluorescent material was held at one end with a split clamp. Excitation illumination was provided by a 100 W xenon lamp + monochromator (Bentham), delivered via a 6 mm diameter fiber bundle. A single 50 mm focal length lens was used to focus the excitation light on to the surface of the strip. The fiber and focusing lens were mounted on an optical rail so the 2 mm diameter illumination spot could be moved along the length of the strip. Excitation wavelengths were 530 nm for R305 and 320 nm for EuhD.

The detection fiber (600 μm diameter, 0.22 NA, Ocean Optics) was mounted in a spring-loaded holder on an *XYZ* micrometer stage and was centered in the end of the strip. An optical coupling medium (glycerine) was initially tried, but it did not affect either the spectral profile or decay rate of intensity with distance. Therefore, no optical coupling medium was used for the experiments reported here. Light from the detection fiber was collected by a spectrometer (Jobin-Yvon iHR320) equipped with a UV/vis photomultiplier tube (Hamamatsu R928).

Table 1. Sample Concentrations Used in Measurements

Dye	Concentration (ppm)	Sample Geometry
R305	5	Strip
R305	98	Strip
R305	197	Strip
R305	295	Strip
R305	393	Strip
R305	787	Strip
R305	1574	Strip
R305	210	Square
EuhD	210	Square

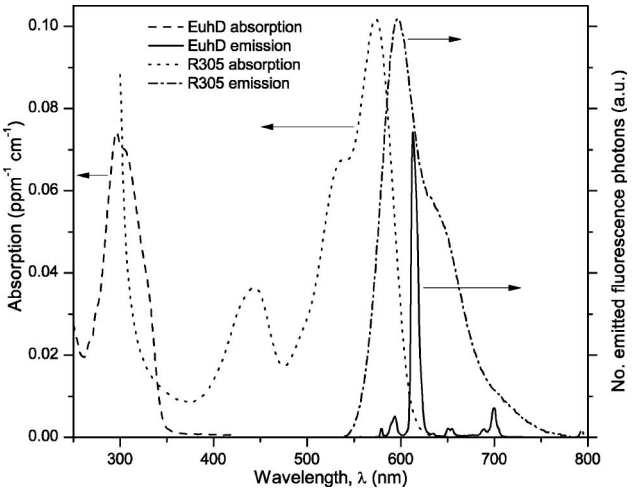

Fig. 2. Absorption and emission spectra of R305 and EuhD. Emission spectra are normalized to the respective peak absorption. Excitation wavelengths for EuhD and R305 are 320 and 530 nm, respectively.

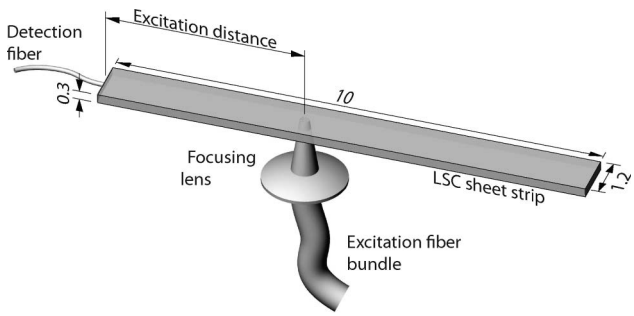

Fig. 3. Measurement of edge emission spectra from a strip of LSC sheet. Dimensions in centimeters.

D. Monte Carlo Simulations

Since the aim of the simulations is to determine the probability that fluorescence photons emitted inside the sheet will reach the edges, we decided to simulate initial fluorescence photons, rather than the more common approach of simulating incident solar photons [27–31]. Although exactly the same results can be obtained from both methods, simulating initial fluorescence photons is somewhat simpler because the program does not need to model either a solar spectrum (to generate incident photons) or the wavelength-dependent surface reflectivity of the LSC sheet. A C++ program was written to generate many initial fluorescence photons at random locations throughout the LSC sheet and follow each of these as they traveled to the edges via internal reflections from the surfaces of the sheet. Host absorption, dye reabsorption, and angular dependence of LSC–air interface reflectivity are all accounted for. The repeatability of the results from the program with an initial number of 2 million photons is $\pm 0.02\%$. Two different sizes of LSC sheets were simulated. The smaller size, 10 cm × 10 cm × 0.3 cm, was chosen because this was a convenient size for casting and on which to perform measurements, while the larger size, 30 cm × 30 cm × 0.3 cm, was chosen as a representative size for a prototype LSC module in which reabsorption effects are more pronounced because of the longer path lengths involved. The program calculates the optical efficiency of the LSC sheet, η_{OPT}, defined as the number of photons emitted at the edges divided by the number of photons absorbed over the surface.

E. Measurement of Optical Efficiency of Luminescent Solar Concentrator Sheets

The percentage of photons trapped in a LSC sheet under uniform illumination can be determined by measuring the number of photons emitted at the edge compared with the number absorbed. This can be done either using a solar cell [27], an integrating sphere [41], or an optical fiber [39]. While simple to use and able to collect light from the entire edge, the solar cell gives no information on the spectral profile of the light emitted or absorbed. The integrating sphere is problematic because of sphere errors and intensity calibration. Therefore, the optical fiber approach is adopted here. The experimental setup is shown in Fig. 4. The 10 cm square sheets were used for this and were clamped vertically on an optical table. Care was taken to ensure that the clamping arrangement did not shade the fluorescent sheet from the illumination.

Two different light sources were used to illuminate the sheet, depending on which dye was under study. The organic R305 dye absorbs mainly in the visible, so a tungsten–halogen lamp was used. However, the EuhD only absorbs in the UV, where the output of a tungsten–halogen lamp is negligible. Therefore, for the EuhD sheets, the lamp shown in Fig. 4 was replaced with a xenon lamp (150 W, Oriel).

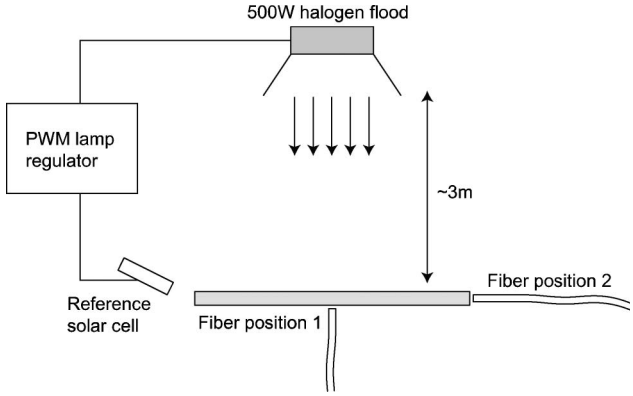

Fig. 4. Measurement of the percentage of photons trapped in a LSC sheet under uniform illumination. The lamp shown was used for measurements on R305 sheets and was replaced with a xenon lamp for EuhD sheets.

The tungsten–halogen lamp was intensity stabilized and was based on a standard 500 W outdoor floodlight with closed-loop control of the intensity. A microcontroller was used to regulate the lamp intensity by pulse-width modulation control of the current. A small solar cell placed near the LSC sheet was used as a reference detector. Lamp stability was 0.02% over 1 h.

The unfiltered output of the xenon lamp was deliberately defocused to ensure uniform illumination across the LSC sheet under study. The output intensity was monitored with a photocell and was found to be sufficiently stable (to ~0.5%), even though the lamp is not intensity regulated.

An optical fiber, coupled to the spectrometer (iHR320), was used to measure both the number of photons absorbed over the surface of the sheet and the number emitted at the edges. The fiber has an acceptance angle of 25.4° in air. Only those photons from the edge of the sheet that are emitted within this acceptance cone can be detected. This is approximately 2.4%, based on the solid angle of the acceptance cone. With the fiber in position 1 (Fig. 4) and the LSC sheet removed, the fiber detects the light directly incident on the front surface of the LSC. The fluorescent sheet is then placed in front of the fiber. The fiber now records the light transmitted through the sheet. Once reflection is corrected for, the difference in these is a measure of the number of photons absorbed by the sheet. The fiber can then be placed in position 2, where it will measure the number of photons emitted at the edge. Corrections are then applied for the acceptance cone of the fiber, the distribution of light intensity along the edge of the sheet [42] (more intense in the middle of the edge), and the slight variation in sheet thickness from corner to corner. This results in values for both the number of photons absorbed over the surface and emitted at the edges. From this, it is then possible to calculate the percentage of absorbed photons that are collected at the edges of the sheet.

3. Results

A. Effect of Excitation Wavelength on Emission Spectrum and PLQY of R305-Doped PMMA

The emission spectrum of the R305 dye in PMMA was measured as the excitation wavelength was varied from 310 to 620 nm in steps of 20 nm. The sample concentration was 5 ppm, sufficiently low to minimize effects of reabsorption within the sample on the observed emission spectrum. Figure 5 shows the measured emission spectra. The results have been separated into two groups depending on the excitation wavelengths chosen and whether any change in the spectral profile was observed. All spectra have been normalized to a peak value of 1.

As the excitation wavelength was increased from 320 to 490 nm [Fig. 5(a)], there was no significant change observed in the shape or wavelength of the emission spectrum. The peak emission wavelength remained fixed at 597 nm. At excitation wavelengths above 490 nm, however, the spectra showed a shift toward progressively longer wavelengths as the excitation wavelength was increased. The peak emission wavelength increased from 597 nm at $\lambda_{ex} = 510$ nm to 611 nm at $\lambda_{ex} = 620$ nm.

Figure 6 shows the measured PLQY at different excitation wavelengths. The sample concentration in this case was 98 ppm, since a higher concentration was required to achieve a detectable signal when using the integrating sphere. Within the error limits ($\pm 2\%$), there is no detectable change in the PLQY as the excitation wavelength is varied.

The intrinsic emission spectrum of the R305 dye molecule must be independent of excitation wavelength, as can be seen from the energy-level diagram in Fig. 1(b). Regardless of the energy of the excitation photon, the excited molecule always relaxes to the lowest vibrational level of S_1 before decaying to a vibrational level of S_0 by emitting a fluorescence photon, resulting in the same emission wavelengths. This is borne out by the invariance of the emission spectrum with excitation wavelength in the range of 310–490 nm. Likewise, the PLQY also remains constant because the emission process is the same.

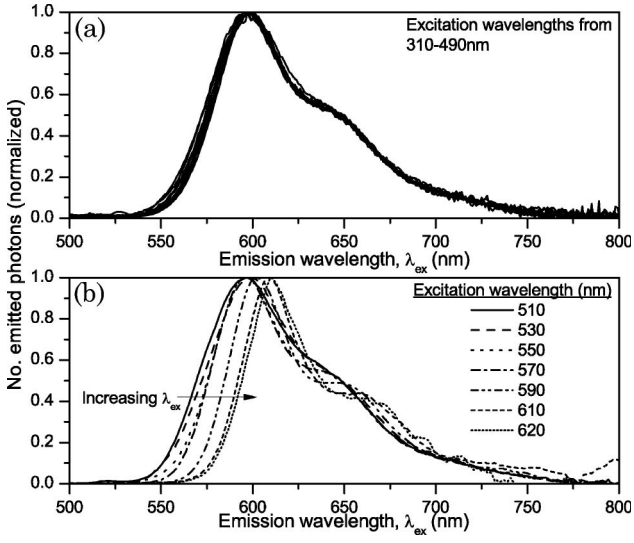

Fig. 5. Emission spectrum of R305 in PMMA (measured from a 5 ppm sample) as excitation wavelength is varied from (a) 310 to 490 nm and (b) 510 to 620 nm.

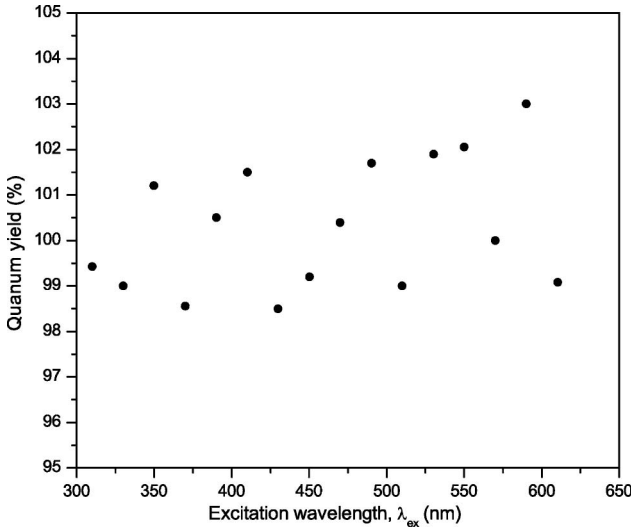

Fig. 6. PLQY of R305 (measured from a 98 ppm sample) versus excitation wavelength.

The change in the emission spectrum that occurs at excitation wavelengths greater than 490 nm can be explained by the presence of aggregated dye molecules, such as dimers or trimers, which have longer emission and absorption wavelengths than the individual (monomer) molecules. As the excitation wavelength is increased, the contribution to the emission spectrum from these aggregates becomes progressively larger, resulting in a redshift of the composite spectrum until, at 620 nm excitation, the observed emission is due entirely to aggregates. The lack of dependence of PLQY on excitation wavelength shows that aggregation does not reduce the PLQY, with a value of near unity being retained. These fluorescence properties, redshifted emission and high PLQY, are characteristic of so-called *J*-aggregates, in which the molecules are stacked with their planes parallel but displaced from a perfect sandwich structure by a longitudinal offset between adjacent molecules. R305 is a member of the perylene bisimide class of dyes. *J*-aggregate formation in nonpolar solvents, such as methylcyclohexane, has been observed previously for perylene bisimide dyes that are similar to R305 in having phenoxy substituents in the "bay area" of the perylene core [43]. In the absence of bulky substituents, such as phenoxy groups, in the bay area, perylene bisimides tend to form sandwich-type *H*-aggregates [44], which show blueshifted absorption spectra and greatly reduced PLQYs, relative to the monomer. These results are significant, because they suggest that the reabsorption losses in a LSC sheet containing the R305 dye will be less than expected from assuming the emission spectrum

is independent of excitation wavelength. Reabsorption of monomer emission at wavelengths on the red edge of the absorption spectrum will result in excitation of redshifted aggregate emission. The emission spectrum resulting from each reabsorption event is thus progressively redshifted, which decreases the probability of subsequent reabsorption.

B. Reabsorption in R305 Luminescent Solar Concentrator Strips

By measuring the profile of the fluorescence spectra emitted from the end of the strip samples at different excitation distances, it is possible to see how the probability of a fluorescence photon reaching the edge varies with excitation distance and dye concentration. The spectra can also be used to accurately determine the tail absorption spectrum of the dye in the sheet.

We define P_0 as the overall probability that a first-generation fluorescence photon (one emitted at the point of excitation) will reach the detector without suffering reabsorption. It is calculated from Eq. (2):

$$P_0 = \frac{\int E'(\lambda)\mathrm{d}\lambda}{\int E(\lambda)\mathrm{d}\lambda}, \tag{2}$$

where $E(\lambda)$ is the molecular emission spectrum of the dye, when the effects of reabsorption are absent, and $E'(\lambda)$ is the spectrum measured from the end of the strip, scaled to match $E(\lambda)$ at long wavelengths where reabsorption is negligible. $E(\lambda)$ was measured from the end of a strip containing a low concentration (5 ppm) of dye, with an excitation distance of only 0.2 cm. The concentration and excitation distance are small enough that any reabsorption effects are negligible (Lakowicz [32], Section 2.8). The normalization procedure used to obtain $E'(\lambda)$ is described briefly below.

Figure 7 shows an example of the spectral normalization procedure for a strip containing 98 ppm of R305 dye, excited at a distance of 5 cm. The raw (unscaled) emission spectrum, $E_{\mathrm{raw}}(\lambda)$, is divided by the molecular emission spectrum, $E(\lambda)$, to obtain the ratio $E_{\mathrm{raw}}(\lambda)/E(\lambda)$. As can be seen in Fig. 7, this ratio levels out above 750 nm and is constant at ~2.53. The ratio becomes constant because reabsorption is no longer occurring appreciably at these wavelengths. If $E_{\mathrm{raw}}(\lambda)$ is then divided by this constant ratio, it is scaled so it matches $E(\lambda)$ exactly at long wavelengths, resulting in $E'(\lambda)$. Using this ratio to scale the spectra is more accurate than scaling them "manually" until they fit.

The shape of the ratio plot is indicative of how far the absorption tail extends into the emission spectrum. Once the edge-emitted spectra have been scaled as described, the probability values P_0 can be calculated using Eq. (2).

The system shown in Fig. 3 was used to measure P_0 for strip samples containing seven different concentrations of R305 dye at excitation distances ranging from 0.2 to 9 cm. The results are shown in Fig. 8. Since P_0 depends on both dye concentration and the excitation distance, it is plotted versus the effective optical density ($\mathrm{OD_{eff}}$) of the path from the excitation point to the detector, calculated from Eq. (3):

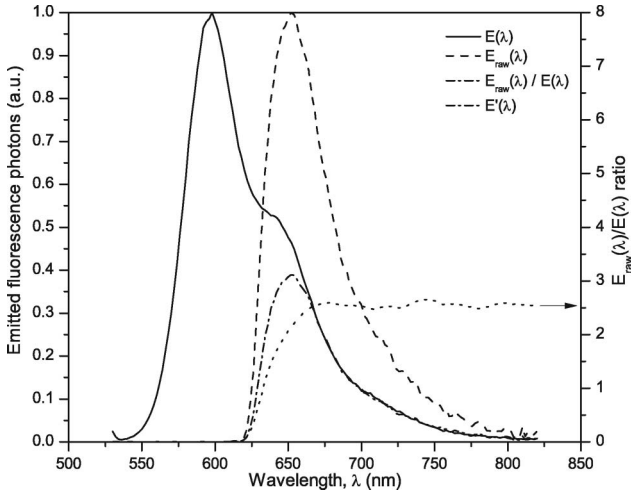

Fig. 7. Example of scaling procedure. Shown are the molecular emission spectrum, $E(\lambda)$, the raw spectrum measured from the strip, $E_{\mathrm{raw}}(\lambda)$, the ratio $E_{\mathrm{raw}}(\lambda)/E(\lambda)$, and the scaled emission spectrum, $E'(\lambda)$, obtained by dividing $E_{\mathrm{raw}}(\lambda)$ by the constant ratio at long wavelengths (0.34).

$$\mathrm{OD_{eff}} = \varepsilon_{\mathrm{peak}} \times c \times d \times \log(2.71828), \tag{3}$$

where $\varepsilon_{\mathrm{peak}}$ is the peak Naperian absorption coefficient of the dye (0.101 $\mathrm{ppm^{-1}\,cm^{-1}}$ for R305 in PMMA), c is the dye concentration in ppm, and d is the excitation distance in centimeters. The logarithmic factor corrects for the different bases used in the definition of optical density and the absorption coefficient. This *effective* optical density is used because the trapped fluorescence light follows a range of diagonal paths between the top and bottom

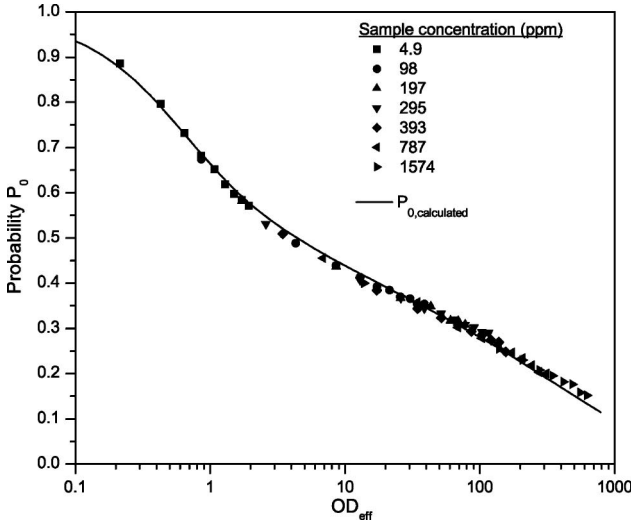

Fig. 8. P_0 versus effective optical density, showing experimental data (points) and calculated curve (curve).

surfaces of the sheet as it travels to the edge, and the actual average path length inside the strip is unknown and different from the excitation distance, although it can be determined from a ray-tracing simulation [39]. By doing this, it becomes possible to calculate a value for P_0 from the molecular emission spectrum, $E(\lambda)$, and the absorption spectrum of the dye, $\varepsilon(\lambda)$, by replacing $E'(\lambda)$ in Eq. (2) with $E(\lambda)e^{-\varepsilon(\lambda)cl}$. This uses the Beer–Lambert law to predict the fluorescence spectrum transmitted through an average path length l of dye-doped material, where the average path length is obtained from the ray-tracing simulation and is a factor of 1.1 to 1.3 times greater than the excitation distance, depending on the dye concentration. This calculated value, $P_{0,\text{calculated}}$, is also plotted in Fig. 8.

Values measured for P_0 from the seven different sample concentrations all show good agreement with each other. For example, P_0 measured from a 393 ppm sample with an excitation distance of 3 cm is identical to that measured from a 197 ppm sample with a 6 cm excitation distance, since OD_{eff} is the same in both cases (half the concentration but twice the distance).

As either excitation distance or dye concentration is increased (both of which result in an increase in the effective optical density), the probability of the photons reaching the detector drops dramatically. At larger distances or higher concentrations, the first-generation fluorescence photons pass through a greater amount of dyed material; therefore, there is an increased chance that they will be reabsorbed by the dye and lost. In addition, as the concentration is increased, the *rate* of decay of probability with excitation distance becomes *less*. For example, the probability decreases more rapidly with a 5 ppm sample than it does with a 393 ppm sample. This is due to increased reabsorption losses at shorter distances in highly concentrated samples. Any photons that survive more than a few centimeters will then suffer little subsequent reabsorption; any reabsorption that is experienced is then due primarily to the low-magnitude absorption tail. It can be seen that the decay of probability with concentration is greater at shorter excitation distances, as most reabsorption will occur within the first few centimeters.

There is good agreement between the experimental data and the calculated values obtained using the Beer–Lambert law. This is perhaps unexpected, as the Beer–Lambert law should not apply when the probability of reemission is high. However, whereas the initially excited fluorescence (excitation wavelength 530 nm) arises from monomer dye molecules, reabsorption tends to excite the J-aggregates so that the reemitted fluorescence has a different, redshifted spectrum. Therefore, the attenuation of the primary, short-wavelength emission can be well approximated by simple absorption because there is little reemission in this short-wavelength region. The Beer–Lambert law can thus be used to model the propagation of light inside the strip.

The fraction of photons lost to reabsorption is significant. For example, the dye concentration of 393 ppm is comparable to what might be used in an actual LSC (a concentration high enough to absorb sufficient incident sunlight over the surface of the sheet [45]). If we consider those photons emitted 5 cm from the edge of the sheet, corresponding to an $\text{OD}_{\text{eff}} = 86$, we can see from Fig. 8 that they have only a 30% chance of reaching a particular location on the edge, with the remaining 70% of them undergoing reabsorption. An important fact to remember is that *average* path lengths in a LSC of dimensions 30 cm × 30 cm, which would be considered a minimum practical size [45], are around 15 cm, much larger than the path lengths studied in Fig. 8.

These results show that the bulk of reabsorption occurs over the first few centimeters of the LSC and, thereafter, the reabsorption is governed by the tail absorption of the dye. This is one of the reasons many of the recently reported record LSC efficiencies [22,46] have been measured from very small (<5 cm) minimodules. By constructing relatively thick modules with such small surface areas, the problems of reabsorption are reduced, but at the cost of dramatically reducing the concentration ratio.

The importance of reabsorption is clear. However, we do not yet know the extent to which the tail of the absorption spectrum overlaps with the emission spectrum. We can easily measure the main part of the absorption spectrum with the UV/vis spectrophotometer and a sheet sample, but to measure the extremely low-magnitude absorption tail would require a much greater sample thickness—for example, 10 cm. Casting samples of this thickness is not easy using the laboratory-scale water-bath technique. However, we can instead use the fluorescence spectra measured from the ends of the strip samples to determine the tail absorption spectrum [39]. If we use $E(\lambda)$ and $E'(\lambda)$ to denote the molecular and scaled emission spectra, as before, then we can calculate an effective tail absorption coefficient of the dye from Eq. (4):

$$\varepsilon_{\text{eff}} = -\frac{1}{cd}\ln\left\{\frac{E'(\lambda)}{E(\lambda)}\right\}, \tag{4}$$

where the dye concentration and excitation distance are represented by c and d, both of which are known. ε_{eff} is expressed in terms of the excitation distance, rather than the average optical path length. Once the tail of the absorption spectrum was calculated in terms of ε_{eff}, it was scaled to match the long-wavelength end of the main absorption spectrum, obtained from the UV/vis spectrophotometer, as shown in Fig. 9, to give the correct value of ε, corresponding to the average optical path length. The data from the UV/vis spectrophotometer (the main absorption spectrum) are valid below 650 nm; above this, the spectrophotometer is not sensitive enough to detect a change in the light intensity transmitted through the sample. Conversely, the data from the strip end

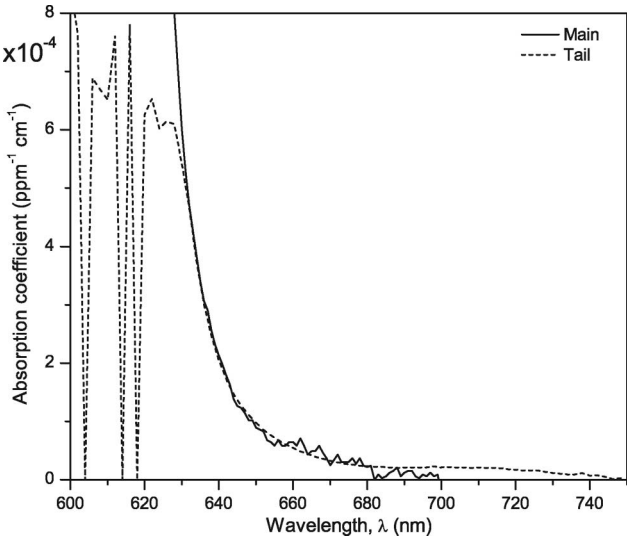

Fig. 9. Scaling of the tail absorption spectrum (measured from the end emission of strip samples) to match the main absorption spectrum (from the UV/vis spectrophotometer) in the range of 630–650 nm.

emission are only valid *above* 630 nm, since little fluorescence is emitted at shorter wavelengths.

The resulting combined absorption spectrum is shown in Fig. 10. The inset shows the tail absorption data obtained from the end emission spectra of the strip samples, calculated using Eq. (4). To reduce the error, several different dye concentrations and excitation distances were used to obtain the tail absorption spectrum and the results averaged.

The tail absorption extends to 750 nm—it may extend further than this, but the magnitude is not significant for the path lengths and concentrations under consideration. For example, the tail absorption data are accurate up to at least 725 nm, where the absorption coefficient is 1×10^{-5} ppm^{-1} cm^{-1}. In a 60 cm × 60 cm × 0.3 cm LSC sheet, which preliminary

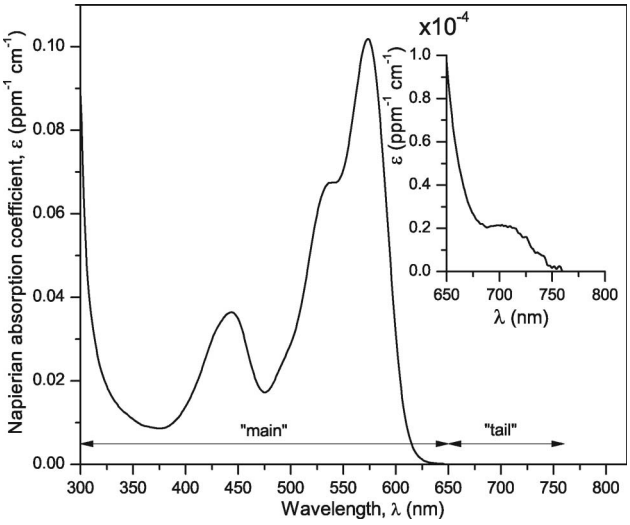

Fig. 10. R305 absorption spectrum in PMMA showing both main and tail absorption regions. A magnified view of the tail absorption is shown in the inset.

simulations have shown results in the lowest module embodied energy, the average path length is 34 cm. For an R305 dye concentration of 350 ppm (an optimum concentration), this results in only 10% absorption. If we refer back to Fig. 2, we can see that nearly all of the R305 emission spectrum lies below 750 nm; in other words, the dye absorbs (to some degree) over its entire emission spectrum. Reabsorption will always be present, no matter how large the path length. This demonstrates the importance of knowing the *entire* absorption spectrum, including the tail, when working with LSCs. Because of the long path lengths involved, a tail absorption that may not be apparent on a UV/vis spectrophotometer scan can have a large impact on the photon transport in the device.

All of the above data relate to point excitation of a strip of LSC material. While this demonstrates photon transport losses at different path lengths, it does not reproduce the performance of a real LSC, which will 1) have illumination over its entire surface and 2) have a much smaller length/breadth aspect ratio. We will next look at the photon transport and losses in both 30 cm square and 10 cm square LSC devices under uniform illumination, using both simulation and experimental measurements.

C. Optical Efficiency of Square Luminescent Solar Concentrator Sheets

The Monte Carlo simulation program was used to model the photon transport inside two different sizes of square LSC sheets containing a range of hypothetical organic dyes with artificially generated emission spectra. The purpose of this study was to examine the effect of different Stokes shifts on the optical efficiency of the sheets. The experimentally measured absorption spectrum of the R305 dye was used in the program and remains fixed throughout. However, the *emission* spectrum was artificially shifted in wavelength to give a range of different Stokes shifts. The peak emission wavelength was shifted from 574 to 800 nm, resulting in Stokes shifts from 0 to 226 nm. The results of these simulations are compared with those for LSCs doped with the the EuhD complex, which exhibits a very large Stokes shift of ~300 nm. First we consider the simulations of the 30 cm square sheet, which show the largest effects of reabsorption, host absorption, and dye PLQY. Results are then shown for a 10 cm square sheet, along with the experimentally measured value for R305 to demonstrate the validity of the simulation.

Figure 11 shows the results for a 30 cm square sheet containing 600 ppm of either the hypothetical dye or EuhD. The Stokes shift of the real R305 dye is 23 nm, indicated by the vertical line.

The calculated η_{OPT} for a sheet containing the EuhD complex is 64% and is shown by the horizontal line in Fig. 11. Since the complex exhibits zero reabsorption, this is simply the product of the probability of an emitted photon being trapped by total internal

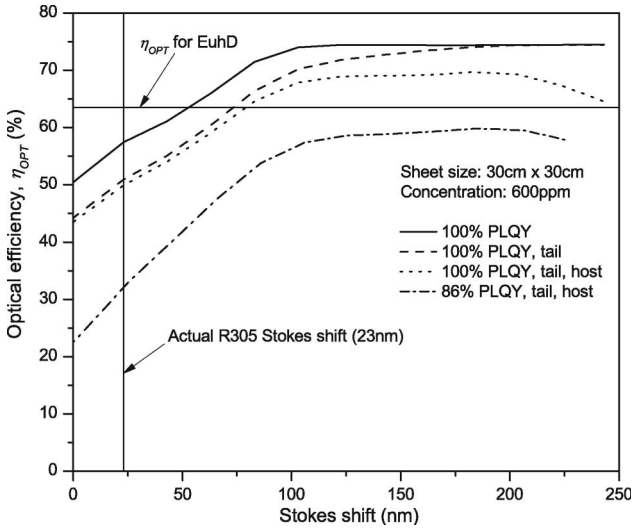

Fig. 11. Simulated η_{OPT} for a 30 cm × 30 cm sheet containing hypothetical dyes with different Stokes shifts, showing the effects of tail absorption, host absorption, and PLQY. Graphs shown are for dye PLQY of 100% with no tail or host absorption (solid curve), dye PLQY of 100% with tail absorption included but no host absorption (dashed curve), dye PLQY of 100% with both tail and host absorption included (dotted curve), dye PLQY of 86% with both tail and host absorption included (dashed-dotted curve). The horizontal line indicates the value of η_{OPT} for the EuhD complex. The vertical line at 23 nm denotes the Stokes shift of the real R305 dye.

reflection, 74% [calculated from Eq. (1)], and the PLQY of the complex, 86%.

Considering first the case where the hypothetical dye has no absorption tail (the absorption is set to zero above 650 nm), there is no host absorption and the dye has 100% PLQY (solid curve in Fig. 11). At Stokes shifts above about 120 nm, η_{OPT} flattens out at 74%. Since there is little spectral overlap and, hence, little reabsorption above this wavelength, this is identical to the fraction of first-generation photons that are emitted at angles outside the escape cone, calculated from Eq. (1). For a refractive index of $n = 1.49$ (PMMA), this is indeed 74%. At smaller Stokes shifts, η_{OPT} drops sharply, as reabsorption begins to occur. Even though the dye has 100% PLQY, each reabsorption/reemission event results in a ~26% chance of the emission photon being directed out of the sheet.

If an absorption tail (from 650 to 750 nm) for the dye is now included in the simulation (dashed curve in Fig. 11), η_{OPT} drops by approximately 7% over the range of Stokes shifts up to 100 nm. This large decrease in η_{OPT}, caused by the presence of an extremely low-magnitude tail, again demonstrates the importance of measuring the tail absorption if accurate predictions are to be made of the optical efficiency.

Inclusion of the host absorption (dotted curve Fig. 11) has the greatest effect at Stokes shifts above 70 nm, corresponding to peak emission wavelengths above 650 nm, where the PMMA begins to show absorption. It leads to an almost 5% decrease in η_{OPT} at a Stokes shift of 200 nm. The two small troughs at Stokes shifts of 150 and 220 nm are due to the peak emission wavelength coinciding with the absorption peaks of PMMA at 730 and 800 nm (caused by CH and CO bond absorption [47]). However, host absorption has little effect on η_{OPT} near Stokes shifts of 23 nm, where the R305 dye emits. This is encouraging, as it suggests that host absorption is not a concern in LSCs that use the R305 dye as the final emitter. For compounds that emit further into the red/infrared, host absorption will have a larger effect.

Under these conditions (100% PLQY, tail and host absorption both included), which correspond to those found in an actual LSC module, η_{OPT} for the (real) R305 dye is 50%. This is less than η_{OPT} for the EuhD complex (64%). Although the latter has a much lower PLQY, this is compensated for by the total absence of reabsorption in the complex. The complex performs better than the organic dye for Stokes shifts up to 50 nm, above which the reabsorption losses of the dye decrease sufficiently to result in a higher η_{OPT}.

It is important to note that η_{OPT} for the R305-doped 30 cm × 30 cm sheet is much higher than the P_0 value calculated from the average path length inside the square sheet. For a 30 cm × 30 cm sheet, the average optical path length is approximately 15.5 cm, determined from simulations, which corresponds to an $OD_{eff} \approx 400$ at an R305 concentration of 600 ppm. Referring to Fig. 8, the corresponding P_0 value at this OD_{eff} is $P_0 \approx 18\%$, considerably lower than the value of $\eta_{OPT} = 50\%$. η_{OPT}, however, describes the percentage of photons detected at *any* location on *any* edge. This contrasts the point excitation/detection method used to determine P_0, where photons from secondary and subsequent emission events will lack a direct path to the detector and not generally contribute.

To demonstrate how critical a high PLQY is for the organic dyes, we now consider the effect of reducing the quantum yield to 86%, the same as the EuhD complex, (dashed-dotted curve in Fig. 11). For a Stokes shift of 23 nm, this reduced PLQY results in a dramatic decrease in η_{OPT} to only 32%. Thus, a small change in PLQY is magnified by the multiple reabsorption/reemission events that occur within the sheet.

Figure 12 shows the same simulations as in Fig. 11 performed on a 10 cm square sheet containing 210 ppm of either hypothetical organic dye or EuhD complex. The effects of reabsorption, host absorption, and PLQY are less pronounced because of the lower dye concentration and shorter path lengths, but they still exist. The EuhD still performs better than the R305.

The experimental system shown in Fig. 4 was used to measure the value of η_{OPT} for 10 cm square LSC sheets containing R305 or EuhD. The measured value of $60 \pm 3\%$ obtained for a sheet containing the R305 dye is shown in Fig. 12 and is in good agreement with the calculated value. The value of η_{OPT} for the EuhD sheet was $60 \pm 3\%$, which is also in good agreement with the calculated value of 64%.

The error bars on the experimental measurement are due to the both the difficulty in correcting for the

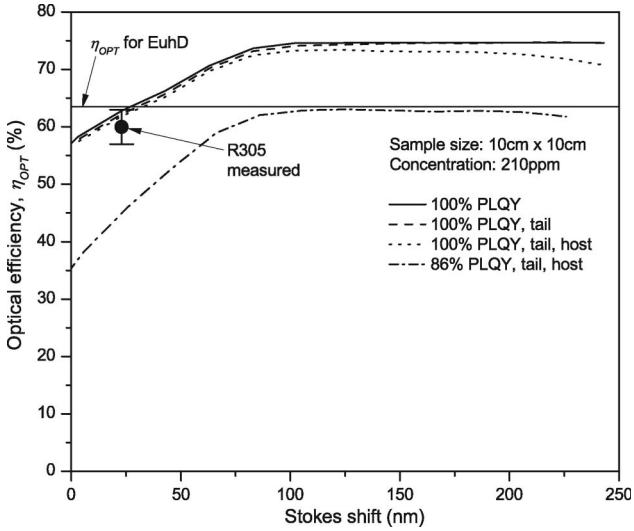

Fig. 12. Simulated (curves) and measured (black circles) η_{OPT} for a 10 cm × 10 cm sheet. For description of each curve, see caption of Fig. 11.

slight nonuniform thickness of the sheet (5% corner–corner) and the noise in the low signal level from the spectrometer (the spectrometer slits had to be set very narrow when the fiber was measuring the incident light, and these slit settings must be kept for the edge measurement as well). Four other concentrations of sheets (70, 197 ppm of R305 and 110, 146 ppm of EuhD) were also measured and exhibited good agreement with simulated values (within 2%).

4. Conclusions

Excitation of the R305 dye on the long-wavelength edge of the absorption spectrum was found to result in emission that was redshifted relative to that excited at shorter wavelengths. Despite the change in emission spectrum, the PLQY was found to be independent of excitation wavelength. These observations indicate the formation of *J*-aggregates by the dye molecules in the PMMA matrix. As a consequence of this, reabsorption of the primary emission will result in the redshift of the emission spectrum, leading to a reduction in the probability of subsequent reabsorption. To our knowledge, this is the first report of dye aggregation in a LSC. However, this is likely to be a widespread phenomenon because the large planar aromatic structures of organic dye molecules that are typically used in LSCs have a high propensity to form stacked aggregates. Although in the present case the aggregates formed are highly fluorescent, it is common for the aggregation of planar dye molecules to result in a large decrease in PLQY.

The long-wavelength tail of the absorption spectrum of the R305 dye was determined and found to extend more than 100 nm beyond the long-wavelength limit measurable by conventional absorption spectrometry. Other dyes in the Lumogen range were also found to exhibit a long absorption tails. When combined with the long path lengths present in LSC modules, the absorption tail makes a significant contribution to the loss of photons by reabsorption (as much as 15% relative loss). Because of the many reabsorption events that occur with an organic dye, the PLQY has a great impact on the optical efficiency. Decreasing the dye PLQY from 100% to 86% results in nearly *halving* the optical efficiency. By contrast, rare-earth complexes, such as EuhD, can outperform the organic dye even though their PLQY is lower, because of the lack of reabsorption. If the absorption wavelengths of rare-earth complexes can be extended into the visible part of the spectrum, then they will be ideally suited for LSC use.

The authors thank Neil Kirtley and Lesley Minto of Lucite International (Wilton, UK) for PMMA sheet casting and supply of casting materials, as well as BASF (Ludwigshafen, Germany) for supplying the Lumogen F dyes used in this research. This research was partially funded by the Engineering and Physical Sciences Research Council (EPSRC) (UK) (grants EP/F02763X and EP/F02732X).

References

1. J. S. Batchelder, A. H. Zewail, and T. Cole, "Luminescent solar concentrators. 1. Theory of operation and techniques for performance evaluation," Appl. Opt. **18**, 3090–3110 (1979).
2. J. S. Batchelder, A. H. Zewail, and T. Cole, "Luminescent solar concentrators. 2. Experimental and theoretical analysis of their possible efficiencies," Appl. Opt. **20**, 3733–3754 (1981).
3. A. Goetzberger and W. Greubel, "Solar energy conversion with fluorescent collectors," Appl. Phys. **14**, 123–139 (1977).
4. A. Goetzberger, "Fluorescent solar energy collectors: operating conditions with diffuse light," Appl. Phys. **16**, 399–404 (1978).
5. W. H. Weber and J. Lambe, "Luminescent greenhouse collector for solar radiation," Appl. Opt. **15**, 2299–2300 (1976).
6. M. Sidrach de Cardona, M. Carrascosa, F. Meseguer, F. Cusso, and F. Jaque, "Outdoor evaluation of luminescent solar concentrator prototypes," Appl. Opt. **24**, 2028–2032 (1985).
7. G. Seybold and G. Wagenblast, "New perylene and violanthrone dyestuffs for fluorescent collectors," Dyes Pigments **11**, 303–317 (1989).
8. J. M. Drake, M. L. Lesiecki, J. Sansregret, and W. R. L. Thomas, "Organic dyes in PMMA in a planar luminescent solar collector: a performance evaluation," Appl. Opt. **21**, 2945–2952 (1982).
9. P. S. Friedman and C. R. Parent, Luminescent Solar Concentrator Development—Final Subcontract Report, contract DE-AC02-83CH10093 (U.S. Department of Energy, 1984).
10. S. J. Gallagher, B. C. Rowan, J. Doran, and B. Norton, "Quantum dot solar concentrator: Device optimisation using spectroscopic techniques," Solar Energy **81**, 540–547 (2007).
11. S. J. Gallagher, B. Norton, and P. C. Eames, "Quantum dot solar concentrators: Electrical conversion efficiencies and comparative concentrating factors of fabricated devices," Solar Energy **81**, 813–821 (2007).
12. D. J. Farrell, A. J. Chatten, A. Buchtemann, and K. W. J. Barnham, "Fabrication, characterisation and modelling of quantum dot solar concentrator stacks," in *IEEE 4th World Conference on Photovoltaic Energy Conversion* (IEEE, 2006), pp. 217–200.
13. V. Pilla, L. P. Alves, E. Munin, and T. T. Pacheco, "Radiative quantum efficiency of CdSe/ZnS quantum dots suspended in different solids," Opt. Commun. **280**, 225–229 (2007).

14. H. Lu and J. Ballato, "Synthesis and characterization of Er^{3+}-doped sol-gel silica containing vanadium oxide nanotubes," J. Am. Ceram. Soc. **89**, 3573–3576 (2006).
15. G. A. Kumar, C. W. Chen, R. Riman, S. Chen, D. Smith, and J. Ballato, "Optical properties of a transparent CaF_2:Er^{3+} fluoropolymer nanocomposite," Appl. Phys. Lett. **86**, 241105 (2005).
16. J. Ballato, R. E. Riman, and E. Snitzer, "Sol-gel synthesis of rare-earth-doped lanthanum halides for highly efficient 1.3 μm optical amplification," Opt. Lett. **22**, 691–693 (1997).
17. R. W. Olson, R. F. Loring, and M. D. Fayer, "Luminescent solar concentrators and the reabsorption problem," Appl. Opt. **20**, 2934–2940 (1981).
18. M. G. Debije, P. P. C. Verbunt, B. C. Rowan, B. S. Richards, and T. L. Hoeks, "Measured surface loss from luminescent solar concentrator waveguides," Appl. Opt. **47**, 6763–6768 (2008).
19. B. C. Rowan, L. R. Wilson, and B. S. Richards, "Advanced material concepts for luminescent solar concentrators," IEEE J. Sel. Top. Quantum Electron. **14**, 1312–1322 (2008).
20. J. Ballato, S. Foulger, and D. W. Smith Jr., "Optical properties of perfluorocyclobutyl polymers," J. Opt. Soc. Am. B **20**, 1838–1843 (2003).
21. Y. Hasegawa, K. Sogabe, Y. Wada, and S. Yanagida, "Low-vibrational luminescent polymers including tris (bis-perfluoromethane and ethanesulfonylaminate) neodymium(III) with 8 coordinated DMSO-d6," J. Lumin. **101**, 235–224 (2003).
22. J. C. Goldschmidt, M. Peters, A. Bosch, H. Helmers, F. Dimroth, S. W. Glunz, and G. Willeke, "Increasing the efficiency of fluorescent concentrator systems," Sol. Energy Mater. Sol. Cells **93**, 176–182 (2009).
23. P. P. C. Verbunt, A. Kaiser, K. Hermans, C. W. M. Bastiaansen, D. J. Broer, and M. G. Debije, "Controlling light emission in luminescent solar concentrators through the use of dye molecules planarly aligned by liquid crystals," Adv. Funct. Mater. **19**, 2714–2719 (2009).
24. O. Moudam, B. C. Rowan, M. Alamiry, P. Richardson, B. S. Richards, A. C. Jones, and N. Robertson, "Europium complexes with high total photoluminescence quantum yields in solution and in PMMA," Chem. Commun. 6649–6651 (2009).
25. S. Biju, D. B. A. Raj, M. L. P. Reddy, and B. M. Kariuki, "Synthesis, crystal structure, and luminescent properties of novel Eu^{3+} heterocyclic beta-diketonate complexes with bidentate nitrogen donors," Inorg. Chem. **45**, 10651–10660 (2006).
26. M. H. V. Werts, R. T. F. Jukes, and J. W. Verhoeven, "The emission spectrum and the radiative lifetime of Eu^{3+} in luminescent lanthanide complexes," Phys. Chem. Chem. Phys. **4**, 1542–1548 (2002).
27. A. Burgers, L. Sloof, A. Buchtemann, and J. van Roosmalen, "Performance of single layer luminescent concentrators with multiple dyes," in *IEEE 4th World Conference on Photovoltaic Energy Conversion* (IEEE, 2006), pp. 198–201.
28. A. R. Burgers, L. H. Slooff, R. Kinderman, and J. A. M. van Roosmalen, "Modelling of luminescent concentrators by ray-tracing," in *Proceedings of the 20th European Photovoltaic Solar Energy Conference and Exhibition* (WIP, 2005), pp. 394–397.
29. M. Carrascosa, S. Unamuno, and F. Agullo-Lopez, "Monte Carlo simulation of the performance of PMMA luminescent solar collectors," Appl. Opt. **22**, 3236–3241 (1983).
30. B. S. Richards and K. R. McIntosh, "Ray-tracing simulations of luminescent solar concentrators containing multiple luminescent species," in *Proceedings of the 21st European Photovoltaic Solar Energy Conference* (WIP, 2006), pp. 185–188.
31. T. J. J. Meyer, J. Hlavaty, L. Smith, E. R. Freniere, and T. Markvart, "Ray tracing techniques applied to modelling of fluorescent solar collectors," Proc. SPIE **7211**, 72110N (2009).
32. J. R. Lakowicz, *Principles of Fluorescence Spectroscopy* (Kluwer Academic/Plenum, 1999).
33. BASF Lumogen F Dyes product datasheets, http://www.dispersions-pigments.basf.com/portal/basf/ien/dt.jsp?setCursor=1_422514 (last accessed 05/01/10).
34. R. Iden and G. Seybold, "Perylene compounds," U.S. patent 4,618,694 (21 Oct. 1986).
35. G. B. Smith and J. B. Franklin, "Sunlight collecting and transmitting system," U.S. patent 5,548,490 (20 Aug. 1996).
36. M. Latva, H. Takalo, V.-M. Mukkala, C. Matachescu, J. C. Rodriguez-Ubis, and J. Kankare, "Correlation between the lowest triplet state energy level of the ligand and lanthanide(III) luminescence quantum yield," J. Lumin. **75**, 149–169 (1997).
37. L. R. Wilson and B. S. Richards, "Measurement method for photoluminescent quantum yields of fluorescent organic dyes in polymethylmethacrylate for luminescent solar concentrators," Appl. Opt. **48**, 212–220 (2009).
38. R. Vieweg and F. Esser, "Polymethacrylate," in *Kunsstoff-Handbuch*, R. Vieweg and F. Esser, ed. (Carl Hanser Verlag, 1975), Vol. IX, pp. 15–23.
39. J. Sansregret, J. M. Drake, W. R. L. Thomas, and M. L. Lesiecki, "Light transport in planar luminescent solar concentrators: the role of DCM self-absorption," Appl. Opt. **22**, 573–577 (1983).
40. A. A. Earp, G. B. Smith, P. D. Swift, and J. Franklin, "Maximising the light output of a luminescent solar concentrator," Solar Energy **76**, 655–667 (2004).
41. M. G. Debije, J.-P. Teunissen, M. J. Kastelijn, P. P. C. Verbunt, and C. W. M. Bastiaansen, "The effect of a scattering layer on the edge output of a luminescent solar concentrator," Sol. Energy Mater. Sol. Cells **93**, 1345–1350 (2009).
42. P. S. Friedman, "Luminescent solar concentrators," Opt. Eng. **20**, 887–892 (1981).
43. F. Wurthner, C. Thalacker, D. Siegmar, and C. Tschierske, "Fluorescent *J*-type aggregates and columnar mesophases of perylene bisimide dyes," Chem. Eur. J. **7**, 2245–2253 (2001).
44. F. Wurthner, "Perylene bisimide dyes as versatile building blocks for functional supramolecular architectures," Chem. Commun. 1564–1579 (2004).
45. L. R. Wilson and B. S. Richards, "High-efficiency dyes for luminescent solar concentrators—photostability, modelling and results," in *Proceedings of the 23rd European Photovoltaic Solar Energy Conference and Exhibition* (WIP, 2008), pp. 510–512.
46. L. H. Slooff, E. E. Bende, A. R. Burgers, T. Budel, M. Pravettoni, R. P. Kenny, E. D. Dunlop, and A. Buchtemann, "A luminescent solar concentrator with 7.1% power conversion efficiency," Phys. Status Solidi (RRL) **2**, 257–259 (2008).
47. J. Ballato, S. Foulger, and D. W. Smith Jr., "Optical properties of perfluorocyclobutyl polymers. II. Theoretical and experimental attenuation," J. Opt. Soc. Am. B **21**, 958–967 (2004).